Fuel 117 (2014) 680–687

Contents lists available at ScienceDirect

Fuel

journal homepage: www.elsevier.com/locate/fuel

A two-zone solar-driven gasifier concept: Reactor design and experimental evaluation with bagasse particles

Michael Kruesi [a], Zoran R. Jovanovic [a,*], Aldo Steinfeld [a,b]

[a] ETH Zurich, Department of Mechanical and Process Engineering, 8092 Zurich, Switzerland
[b] Paul Scherrer Institute, Solar Technology Laboratory, 5232 Villigen PSI, Switzerland

HIGHLIGHTS

- Two-zone solar-driven gasifier offers high conversion and favorable syngas quality.
- A drop-tube zone provides efficient radiative heat transfer for rapid pyrolysis.
- A trickle-bed increases solids residence time and enhances the overall heat transfer.
- The two-zone reactor prototype demonstrated improved performance over the drop-tube.
- Solar energy was stored in the syngas and the biomass was energetically upgraded.

ARTICLE INFO

Article history:
Received 10 July 2013
Received in revised form 4 September 2013
Accepted 5 September 2013
Available online 18 September 2013

Keywords:
Gasification
Pyrolysis
Biomass
Solar
Syngas

ABSTRACT

A two-zone solar reactor concept for the steam-based gasification of biomass particles using concentrated solar energy has been developed and experimentally evaluated with particles of sugarcane bagasse at a 1.5 kW solar input scale. The gasifier has been designed with the objective to provide pyrolysis and gasification conditions yielding high carbon conversion into syngas and suppressing the formation of tars and gaseous hydrocarbons. It consists of two zones. In the upper drop-tube zone, a high radiative heat flux to the dispersed particles induces their fast pyrolysis. In the lower trickle bed zone, a structured packing provides the residence time and temperature required for the char gasification and the decomposition of the other pyrolysis products.

A series of 20 min gasification experiments comparing the two-zone reactor vs. a drop-tube reactor were performed in a high-flux solar simulator with a maximum particle flux of 16 g/s m^2. It has been demonstrated that the former allows for more efficient decomposition of CH_4 and C_2 hydrocarbons at comparable reactor temperatures. The LHV of the product gas leaving the two-zone gasifier was significantly higher than those typically obtained in conventional autothermal gasifiers. Solar energy was chemically stored in the product gas, resulting in energetic upgrade of the biomass by 5% and a maximum energy conversion efficiency of 21%.

© 2013 Elsevier Ltd. All rights reserved.

1. Introduction

Solar-driven steam-based gasification of biomass is a promising route for producing precursors for valuable chemicals and low-carbon footprint transportation fuels from a renewable resource [1,2]. The highly endothermic thermochemical conversion of biomass with steam to syngas (a mixture composed of H_2 and CO) comprises two main steps: (1) pyrolysis, producing tars, gases and char, and (2) steam-based gasification of the tars and the char to form syngas [3]. The produced syngas can then be processed into H_2 (water–gas shift reaction), diesel or kerosene (Fischer–Tropsch process), or methanol and then gasoline (MTG, Mobil). Alternatively, the syngas may be used directly as a combustion fuel for power generation.

Previous investigations of solar-driven allothermal gasification of Brazilian sugarcane bagasse have revealed potential benefits over the conventional autothermal gasification such as a higher heating value and a more favorable quality of the produced syngas, i.e. a higher H_2/CO ratio and less CO_2 contamination [4]. Moreover, a higher utilization of the feedstock can be achieved: instead of combusting 25–40% of the feed biomass to provide the heat necessary to drive the endothermic gasification reactions, the solar-driven gasification uses concentrated solar radiation as the source of high-temperature process heat [1,2,4]. Thus, as the solar energy is chemically stored in an amount equal to the enthalpy change of the endothermic reactions, the calorific value of the syngas produced per unit of feedstock is higher.

---

* Corresponding author. Tel.: +41 446325961.
E-mail address: zjovanovic@ethz.ch (Z.R. Jovanovic).

0016-2361/$ - see front matter © 2013 Elsevier Ltd. All rights reserved.
http://dx.doi.org/10.1016/j.fuel.2013.09.011

Nomenclature

ΔH_R	reaction enthalpy (J/mol)
ID	inner diameter (mm)
L	length (mm)
LHV	lower heating value (MJ/kg)/(MJ/Nm^3)
M	molar mass (kg/mol)
m	mass(kg)
$\dot{n}$	molar flow rate (mol/s)
OD	outer diameter (mm)
$\dot{Q}$	heat flow (W)
T	temperature (K)
t	time (s)
U	upgrade factor (–)
x	elemental molar ratios of H/C (–)
X_C	carbon conversion (–)
y	elemental molar ratios of O/C, mole fraction (–)/(–)
η	energy conversion efficiency (–)

Oxygen- and air-blown downdraft gasifiers are the preferred concepts for the autothermal conversion of a highly volatile feedstock such as biomass into a high-quality syngas. They feature a turbulent oxidation zone maintained at temperatures in the range of 1000–1200 °C. While passing through this high-temperature zone, tars and gaseous hydrocarbons released during pyrolysis are cracked and reformed so that the resulting product gas contains low amounts of tars, dust, and CH_4 (~1–2%). However, it is also diluted by a substantial amount of CO_2 and N_2 if air is used as the combustion gas [3] and contaminated by combustion byproducts (SO_x and NO_x) that deactivate catalysts used in the subsequent liquid fuel production step. Therefore, purifying the final product (syngas) and eliminating its dilution imposes additional capital and operating costs for gas scrubbing, CO_2 removal, and on-site O_2 generation.

For solar-driven gasification, where no heat is generated within the reactor, efficient transfer of the concentrated solar radiation to the reaction site is critical for high productivity and favorable gas-phase selectivity. Directly-irradiated solar gasifiers, where the solar radiation is absorbed by the feedstock at the reaction site, enable high heat transfer rates. Yet, those also require a transparent window that not only has to be kept clean during operation which impairs operability in case of highly volatile feedstocks, but also introduces limitations in the scale-up [5–13]. In indirectly-irradiated reactors the incident solar radiation impinges on the outer wall of an opaque absorber which confines feedstock. The heat is transferred to the inner absorber wall by conduction and from there to the feedstock by convection and radiation. Therefore, the need for a window is eliminated at the expense of having less efficient heat transfer. This imposes even more stringent constraints on the materials of the absorber with regards to its operating temperature, chemical stability, thermal conductivity, radiative absorptance, and resistance to thermal shock [2,12,14–20].

A commonly suggested method to achieve the required heat transfer rates in an indirectly-irradiated gasifier is the drop-tube concept. Solar radiation is concentrated through an aperture into either a specularly reflecting [14,19] or absorbing [15,18–20] cavity-receiver housing one or more vertical reactor tubes. The reactor tubes absorb the high-flux irradiation and re-radiate the heat to the particles flowing through. Scalability is straightforward as it is based on a modular multi-tube design [15,21]. However, this reactor concept is suitable only for particles of up to a couple of hundred microns in size for which the radiative heat transfer mode is dominant [22] and the residence time of the order of a second is long enough [4]. Grinding raw biomass to this size range imposes high capital and operating costs that often justify a partial low temperature pyrolysis of the biomass (torrefaction) in order to improve its grindability [23]. At the same time, as the gas is mainly convectively heated by the surface area of the particles that are in a rather dilute flow, this kind of reactor generally does not provide gas temperatures high enough for effective tar and methane cracking and reforming. Alternative reactor concepts such as packed or moving beds allow the use of coarser biomass particles by providing reaction time that is sufficiently long for high carbon conversion. Unfortunately, these concepts suffer from significantly impaired overall heat transfer due to high extinction of radiation by the densely packed bed of feedstock and ash [13,17].

This work introduces a two-zone solar-driven gasifier designed to retain the advantage of the efficient radiative heat transfer inherent to drop-tube reactors while, however, overcoming their residence time and particle size limitations that constrain cracking and reforming of hydrocarbons. The gasifier consists of a drop-tube zone for fast pyrolysis and a trickle bed for the char gasification. The trickle bed utilizes a structured packing to control the overall porosity of the gasification zone in order to increase the residence time of the char particles while still allowing the radiation to penetrate through. The performance of the two-zone reactor was experimentally tested with Brazilian sugarcane bagasse particles and compared to the performance of the drop-tube configuration.

2. Experimental

2.1. Feedstock

The feedstock considered was Brazilian sugarcane bagasse. It was dried (105 °C, >4 h) and sieved (sieve size 0.5 mm) to a mean particle size of 455 μm (LA-950 analyzer, HORIBA). The elemental analysis of the particles presented in Table 1 implies $CH_{1.665}O_{0.663}$ as the overall chemical formula after neglecting the presence of ash, N and S. Calorimetric measurements of the particles after drying (C7000, IKA-Werke) showed a lower heating value (LHV) of 16.50 MJ/kg.

2.2. Solar reactor concept

The biomass pyrolysis conditions such as heating rate, gas temperature, and residence time have a strong influence on the release

Table 1
Elemental analysis of bagasse particles (dry basis); C, H, N determined with CHN-900, O with RO-478 and S with CHNS-932 (all LECO Corporation, St. Joseph, MI).

Bagasse		
Carbon (C)	($\%_{wt}$)	42.51
Hydrogen (H)	($\%_{wt}$)	5.94
Oxygen (O)	($\%_{wt}$)	37.54
Nitrogen (N)	($\%_{wt}$)	0.41
Sulfur (S)	($\%_{wt}$)	0.09
Ash	($\%_{wt}$)	13.5
H/C = x	(mol/mol)	1.665
O/C = y	(mol/mol)	0.663

of tars and gases, as well as on the formation and reactivity of the char. In general, the release of volatiles is enhanced and char formation suppressed by rapid high-temperature pyrolysis [24,25]. Such pyrolysis conditions yield only low amounts of char that has high reactivity [26–29]. Moreover, high gas temperatures facilitate cracking of tars and other hydrocarbons [27,30–32]. Although the production of char with a high reactivity is beneficial for the subsequent char gasification, the char gasification remains the rate limiting step [3]. Previous investigations with the feedstock under consideration indicated that a residence time as high as 30–60 s is required for 90% char conversion at temperatures below the ash melting temperature (1473 K) [4].

The solar gasifier concept developed in this work is based on a vertical tubular reactor situated within a cavity-receiver (Fig. 1). Cavity-type receivers are suitable for solar concentrating applications as they approach blackbody absorbers and minimize re-radiation losses, while providing a homogeneous temperature distribution through multiple internal reflections and re-radiation [33]. The tubular reactor comprises two zones (see inlay Fig. 1): an upper drop-tube pyrolysis zone and a lower trickle-bed gasification zone consisting of a structured packing. Bagasse particles and steam are both introduced from the top. The raw bagasse particles are rapidly heated in the upper zone by infrared radiation from the tube wall to undergo fast pyrolysis. This zone provides sufficient residence time to ensure that the particles reaching the trickle bed are not sticky thus prone to clogging the porous structure. The trickle bed slows down the particles, thus increasing their residence time in the hot zone. Yet, its high overall porosity lets thermal radiation penetrate through, enhancing radial heat transfer. Therefore, by combining conductive and radiative heat transfer modes, the structure is expected to enhance heat transfer to both gas [34] and solid phases. By transporting gas and solids downwards, the tars and gases evolved during the pyrolysis pass through the hottest zone of the reactor where they decompose via cracking and reforming reactions to H_2, CO, CO_2, lighter hydrocarbons and coke.

Together with the potential advantages mentioned above, the concept proposed in this work introduces some limitations that need to be recognized. Although high temperatures are desirable for efficient heat transfer to gas and solids resulting in high reaction rates, the operating temperature of the trickle zone is limited by the ash melting temperature of the feedstock. In addition, the throughput of the feedstock depends on how well the particle loading and residence time within the structured packing can be controlled.

2.3. Experimental setup

The reactor was made of a heat-resistant, well conducting (30 W/m K at 1500 K) pressureless-sintered silicon carbide tube (Hexoloy SE SiC, Saint Gobain, L 700 mm, ID 41 mm, OD 51 mm) which was placed in a cavity (200 × 86 × 86 mm) made of a 60 mm thick (40 mm at the front) alumina/silica based insulation (65% Al_2O_3, 34% SiO_2, Insulform 1600). The insulation was fastened by a stainless steel case surrounding it. The cavity has a 30 mm-diameter aperture for the access of concentrated solar radiation. The reactor tube was placed slightly towards the back of the cavity to reduce thermal stress on the tube and minimize re-radiation losses due to hotspots [19]. A 3-dimensional, water-cooled compound parabolic concentrator (CPC) [35] was mounted as a secondary concentrator at the reactor aperture to boost the concentration ratio, thereby allowing a smaller aperture size and thus further reducing re-radiation losses. The CPC was made of polished aluminum and designed for a half acceptance angle of 45° with an exit diameter of 30 mm. It was truncated to a height of 32.2 mm resulting in an inlet diameter of 42.3 mm and a concentration ratio close to 2. To prevent overheating of the outer surface of the assembly by spilled radiation, a water-cooled shield (300 × 300 mm) was mounted around the CPC. The system was designed for 1.5 kW_{th} solar radiative input power and operation at ambient pressure and temperatures up to 1850 K.

Fig. 2 presents an overview of the experimental setup including the solar gasifier and auxiliary components. Bagasse particles were introduced by an Ar-purged drum feeder positioned above the rector tube. N_2 and steam generated with an external evaporator (Bronkhorst) were injected through annularly distributed inlets positioned just below the feeder. The flow rates of the inlet gases and the water into the evaporator were controlled with electronic mass flow controllers (Bronkhorst). The porous structure creating the trickle bed was made of a 10 ppi (pores per inch) Si–SiC reticulate porous ceramic foam (RPC, porosity >87%) which was placed in the hot zone of the reactor tube. The RPC was supported by an alumina tube (Alsint 99.7, Haldenwanger, ID 30 mm, OD 38 mm).

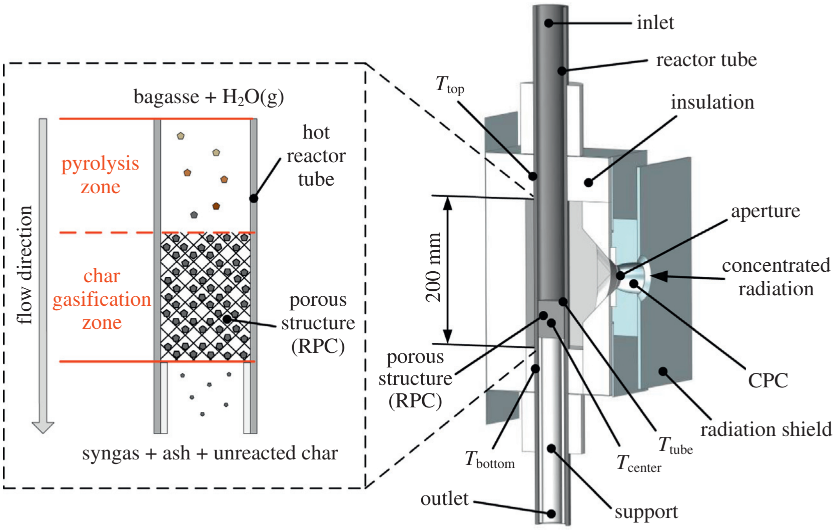

Fig. 1. Schematic of the solar cavity-receiver/reactor configuration with thermocouple locations and blown up detail of the reactor tube showing the fast pyrolysis drop-tube zone and the trickle-bed char gasification zone. (RPC = reticulate porous ceramic, CPC = compound parabolic concentrator).

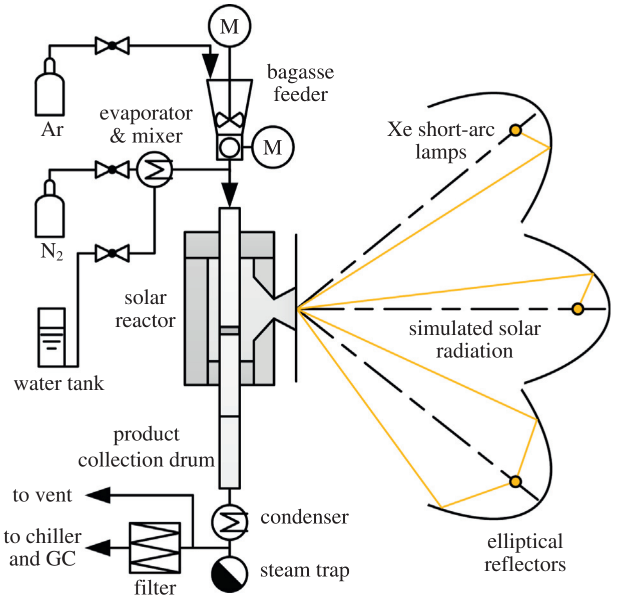

Fig. 2. Schematic of the solar-driven biomass gasifier, including the high-flux solar simulator and the auxiliary components and flows.

The temperatures of the cavity and of the reactor tube wall were measured with K-type thermocouples placed at several axial locations inside the assembly (T_{inlet}, T_{top}, T_{tube}, T_{bottom}, T_{outlet}). One thermocouple (T_{center}) was inserted into the RPC with its tip at the centerline, 20 mm above the bottom of the RPC.

Ash and unreacted char were collected in the product collection drum located below the reactor just before a condenser and a steam trap. A slip-stream of the product gas was withdrawn after the condenser and analyzed by gas chromatography (GC) after being filtered and chilled to remove particulate matter and condensable components. A two-channel Varian Micro-GC equipped with a Molsieve-5A and a Poraplot-U column (1/120 Hz sampling frequency) was capable of determining concentrations of H_2, N_2, CO, CH_4, CO_2, C_2H_2, C_2H_4, and C_2H_6. A known flow rate of N_2 introduced with the steam was used as tracer gas to calculate the total molar flow rate of the product gas.

The experiments were carried out at the high-flux solar simulator (HFSS) of ETH Zurich. The HFSS is equipped with seven high-pressure Xe arcs close-coupled to truncated elliptical specular reflectors [36]. It is capable of delivering continuous thermal radiative power with peak flux intensities up to 4500 suns (1 sun = 1 kW/m^2) and mean flux intensities of 3620 kW/m^2 on a 30 mm aperture diameter. Thus, the solar reactor was tested under comparable heat-transfer characteristics of highly concentrating solar systems, such as solar dishes and solar towers. Radiative flux intensities were adjustable by the number of Xe arcs in operation, their power, and the position of the reactor aperture relative to the focal plane. The radiative power input at the reactor aperture ($\dot{Q}_{solar}$) was determined optically with a calibrated CCD camera and verified by calorimetric measurements at the CPC outlet.

2.4. Experimental procedure

Power input and temperature traces recorded during a typical experiment are shown in Fig. 3. At the beginning of all the experiments but one, the nominal Ar and N_2 flow rates were set to 0.5 L_N/min[1]: in the reference experiment with pure pyrolysis (no steam injection) the nominal flow rates of Ar and N_2 were set to 0.5 L_N/min and 2.2 L_N/min, respectively. In order to achieve rapid heating, up to five arcs of the HFSS were then turned on simultaneously to irradiate the reactor at high power levels (1.65 kW_{th}, 2333 suns). After approximately 30 min, the input power was reduced to the levels ranging between 1.147 and 1.195 kW_{th} (1622–1690 suns) to equilibrate the reactor in a steady-state with the resulting temperature inside the RPC (T_{center}) settling within 1256–1362 K range. The maximum temperature at the top of the RPC at the tube (T_{tube}) was kept below 1428 K to avoid ash slagging that has been observed at temperatures above 1473 K [4,37,38]. After the thermal equilibration of the system, steam preheated to about 560 K was injected at a steady rate of 81.6 g/h resulting in a nominal inlet steam concentration of 62.9%$_{vol}$. The injection of steam ① was reflected by a temperature drop in the upper part of the reactor (T_{top}) and an increase towards the bottom (T_{bottom}). After reaching another steady state, the biomass feed commenced ② at feeding rates between 61 and 94 g/h leading to molar steam to biomass ratios ($\dot{n}_{H_2O}/\dot{n}_{CH_xO_y}$) of 1.37–2.09. This corresponds to 2.06–3.15 times the stoichiometric amount of steam for the idealized net reaction represented by:

$$CH_xO_y + (1-y)H_2O \rightarrow \left(1+\frac{x}{2}-y\right)H_2 + CO \quad (1)$$

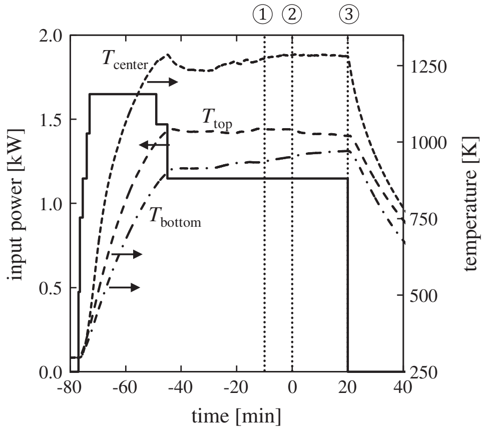

Fig. 3. Input power ($\dot{Q}_{solar}$) and reactor temperatures during a typical experiment; ① steam on, ② biomass feed on and ③ biomass feed off.

After another 20 min, biomass feed, steam flow, and irradiation were all turned off and the reactor was cooled down ③. Temporal gas composition, temperature, and pressure data were acquired during the course of the experiment. In addition, char samples were collected after the experiments and analyzed for their elemental composition (CHN-900, LECO Corporation, St. Joseph, MI).

3. Results and discussion

Fig. 4 shows the molar flow rates of the product gases as a function of time during a typical experimental run. A slight increase in H_2 and CO can be observed immediately after the commencement of steam ①. This has been attributed to the gasification of the carbon residue in the RPC originating from previous experiments. As the step changes in product flow rates could be correlated with turning the biomass feed on ② and off ③, the observed fluctuations in the data shown in Fig. 4 reflect the intermittent feed rate. In addition, the data indicate an increase in the production of H_2 and CO_2 and a decrease in the production of CO, CH_4 and C_2H_4 with time. This could be explained by two factors: (1) the gradual increase in the temperature at the bottom of the cavity as indicated by Fig. 3 and (2) a suspected buildup of char within the RPC. As a result of the char buildup, more syngas is being produced within the RPC that then undergoes the water–gas shift and hydrocarbon

---

[1] L_N designates normal liters at 273 K and 1 atm.

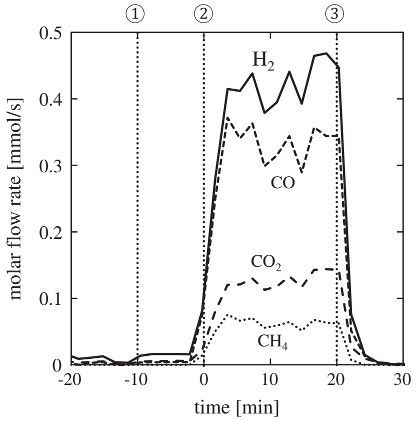

Fig. 4. Molar flow rates of product gases as a function of time during a typical experimental run: ① steam on, ② biomass feed on and ③ biomass feed off.

cracking reactions favored by a higher temperature at the bottom of the cavity.

Experiments were carried out with different system configurations as summarized in Table 2. Two-zone experimental sets A1–A3 and B1–B3 were performed with RPCs that were 50 mm and 100 mm tall, respectively. As reference runs simulating the drop-tube concept alone, free-fall pure pyrolysis (PP) and free-fall steam-based gasification (SG) experiments were performed without any RPC in the system. Furthermore, the experiments were performed at two levels of T_{center}: ~1350 K for set A, SG and PP, and ~1290 K for set B. The observed temperature variations within experimental sets A and B are the result of the physical limitations to strictly control the power input to the solar reactor.

The tabulated mole fractions were calculated considering only molar flow rates of the product gases integrated over the course of an experiment; the flow rates of H_2O, N_2, and Ar were not considered. These were then used to calculate the mass fractions $x_i = y_i M_i / \Sigma(y_i M_i)$ and reported LHV values as follows:

$$\mathrm{LHV} = \sum x_i \, \mathrm{LHV}_i \tag{2}$$

The upgrade factor U is defined as the ratio of the energy content of the syngas produced to that of the reacted bagasse [4] by considering char as pure carbon ($\mathrm{LHV}_{char} = 33.5$ MJ/kg [39]),

$$U = \frac{m_{syngas}\ \mathrm{LHV}_{syngas}}{m_{bagasse}\ \mathrm{LHV}_{bagasse} - m_{C,in}(1 - X_C)\ \mathrm{LHV}_{char}} \tag{3}$$

Table 2

Summary of the experimental results (A = 50 mm tall RPC, B = 100 mm tall RPC, PP = free-fall pure pyrolysis, SG = free-fall steam-based gasification, all values are on a H_2O, N_2 and Ar free basis).

		A1	A2	A3	B1	B2	B3	SG	PP
$\overline{T}_{center}$	(K)	1344	1359	1362	1303	1284	1285	1343	1338
$\overline{T}_{top}$	(K)	1098	1105	1108	1045	1027	1028	1080	1110
$\overline{T}_{bottom}$	(K)	1024	1037	1040	980	965	980	1068	1053
y_{H_2}	($\%_{vol}$)	45.8	46.0	46.5	45.0	43.7	45.0	37.2	35.1
y_{CO}	($\%_{vol}$)	33.8	34.7	34.1	34.8	34.8	34.4	39.9	46.5
y_{CH_4}	($\%_{vol}$)	5.9	5.7	5.4	6.2	6.6	6.3	8.7	7.0
y_{CO_2}	($\%_{vol}$)	13.2	12.5	13.0	12.8	13.2	13.2	10.9	6.2
$y_{C_2H_2}$	($\%_{vol}$)	1.0	0.8	0.8	0.8	1.1	0.6	2.0	3.7
$y_{C_2H_4}$	($\%_{vol}$)	0.4	0.3	0.3	0.4	0.6	0.5	1.1	1.5
$y_{C_2H_6}$	($\%_{vol}$)	0.0	0.0	0.0	0.0	0.0	0.0	0.0	0.0
LHV	(MJ/kg)	15.9	15.9	15.7	15.9	15.9	15.8	17.0	18.5
U	(–)	1.06	1.04	1.06	1.05	1.04	1.05	0.99	1.00
X_C	(–)	0.89	0.80	0.90	0.89	0.90	0.88	0.69	0.64

The carbon conversion X_C is defined as the amount of carbon evolved with monitored product gases divided by the amount of carbon fed with bagasse:

$$X_C = m_{C,product} / m_{C,reactant} \tag{4}$$

Carbon mass balance showed that between 89% and 98% of the total carbon fed into the system could be accounted for by the gas phase evolved over the course of an experiment and the solids recovered from the RPC and the product collection drum. The remainder was attributed to deposits on the tube wall, carryover of fine particles or tar, and the overall measurement error. The fraction of the carbon retained within the RPCs was less than 2.3% and 5.3% for the configurations A and B, respectively.

The statistical significance of the differences between the responses of the investigated configurations has been assessed as follows:

(a) The responses of configurations A and B were compared using two-sample *t*-tests at a significance level of 5% (MATLAB, MathWorks). The variances of the unpaired samples were considered to be equal as confirmed by two-sided *F*-tests at a 95% confidence level.

(b) The single responses of configurations SG and PP were compared to the responses of configurations A and B by single-sided Grubb's outlier tests [40] at a 5% confidence level. These tests were used to decide with 95% confidence if the responses of configurations SG and PP do not belong to the same normal distributions as the corresponding responses of sets A1–A3 and B1–B3.

The results of the statistical analysis are summarized in Table 3. For a comparison X vs. Y, "**>**" or "**<**" designate statistically significant higher or lower response value for configuration X; "~" designates no statistically significant difference.

Fig. 5 presents a comparison of the gas compositions measured with the different system configurations. The average gas mole fractions calculated for the experiments A1–A3 and B1–B3 correspond to H_2/CO ratios of 1.35 and 1.29, respectively, and the same CO_2/CO ratios of 0.38. Although the temperatures ($\overline{T}_{center}, \overline{T}_{top}, \overline{T}_{bottom}$) in set B were on average 59–70 K lower than in set A, according to Table 3 only the mole fractions of H_2 and CH_4 were found to be statistically different.

As shown in Table 3, the comparison of the two-zone configurations A and B to the free-fall pure pyrolysis (PP) indicates a significant decrease in CO, C_2H_2, and C_2H_4 as well as an increase in H_2 and CO_2. The comparison to the free-fall steam-based gasification experiment (SG) indicated the following:

Table 3

Summary of the statistical analysis for the effects of reactor configurations: for comparison X vs. Y "**>**" or "**<**" designate statistically higher or lower mean of a response for the configuration X; "~" designates no statistically significant difference.

Response	A vs. B*	A vs. SG**	B vs. SG**	A vs. PP**	B vs. PP**
y_{H_2}	**>**	**>**	**>**	**>**	**>**
y_{CO}	~	**<**	**<**	**<**	**<**
y_{CH_4}	**<**	**<**	**<**	~	~
y_{CO_2}	~	~	**>**	**>**	**>**
$y_{C_2H_2}$	~	**<**	~	**<**	**<**
$y_{C_2H_4}$	~	**<**	~	**<**	**<**
$y_{C_2H_6}$	–	–	–	–	–
LHV	~	**<**	**<**	**<**	**<**
U	~	~	**>**	~	**>**
X_C	~	~	**>**	~	**>**

* Two-sample *t*-tests at a significance level of 5% with equal variances of the unpaired samples.

** Single-sided Grubb's outlier tests [40] at a 5% confidence level.

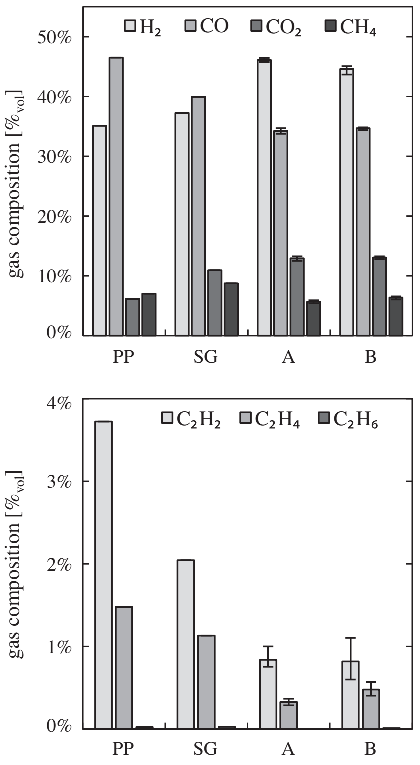

Fig. 5. Average gas compositions calculated on H_2O, N_2 and Ar free basis for the investigated configurations: A = 50 mm tall RPC, B = 100 mm tall RPC, PP = free-fall pure pyrolysis, SG = free-fall steam-based gasification. Error bars illustrate the span between the minimum and maximum values.

- The amounts of CO and CH_4 obtained with either of the two-zone configurations (A, B) were lower and the amount of H_2 higher.
- The amounts of C_2H_2 and C_2H_4 obtained with configuration A were lower but those obtained with configuration B showed no significant difference, and
- The amount of CO_2 obtained with configuration B was higher but the one obtained with configuration A showed no significant difference.

The above observations imply that the two-zone reactor concept allows for more efficient decomposition of CH_4 and C_2 hydrocarbons compared to the drop-tube gasifier operating at comparable reactor tube temperatures. At present, it is not clear whether this should be attributed to a higher gas temperature, an increased residence time of the gas, or both. In addition, it appears that the two-zone reactor facilitates the water–gas shift reaction ($CO + H_2O \leftrightarrow H_2 + CO_2$) which may be attributed to the higher gas temperatures as no effort has been made to quench the product gas. The higher extent of the exothermic water–gas shift reaction with increased gas temperatures is to be attributed merely to faster kinetics as the measured concentrations of H_2 and CO_2 were still below the values expected from thermodynamic equilibrium [41].

The LHVs of the syngas were 15.9 MJ/kg (12.5 MJ/Nm^3) for configurations A and B, and 18.5 and 17.0 MJ/kg (15.6 and 14.4 MJ/Nm^3) for PP and SG, respectively. The statistically higher values for PP and SG originate from the higher content of light hydrocarbons. For all cases, however, the heating values achieved in this work were substantially higher than those obtained in conventional autothermal bagasse gasification. For example, the air-blown cyclone particle-gasifier by Gabra et al. [42] and the air-blown downdraft gasifier for bagasse pellets by Erlich and Fransson [43] produced syngas with an LHV of 4.8–8.1 MJ/Nm^3 and 9.5 MJ/Nm^3, respectively. For comparison reasons, all LHVs are reported on a H_2O and N_2 free basis. The higher values obtained in the solar gasification were mainly due to the lower content of CO_2.

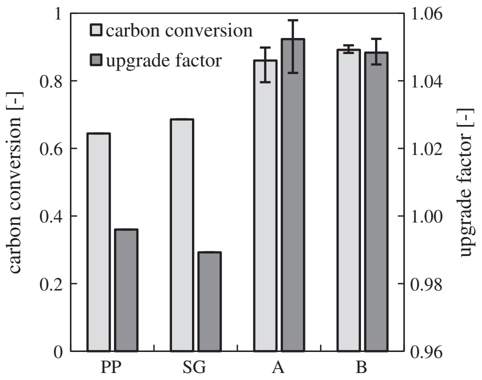

Fig. 6. Carbon conversion and upgrade factors for investigated configurations: A = 50 mm tall RPC, B = 100 mm tall RPC, PP = free-fall pure pyrolysis, SG = free-fall steam gasification. Error bars illustrate the span between the minimum and maximum values.

Carbon conversions (X_C) and upgrade factors are presented in Fig. 6. The carbon conversions for configurations A and B were calculated to be around 87% and 89%, respectively. For B, this is a statistically significant improvement over both PP (64%) and SG (69%), in spite of the considerably lower reactor temperatures. Remarkably, the improvement for configuration A could not be shown to be significant by the Grubbs test due to the scatter in the data

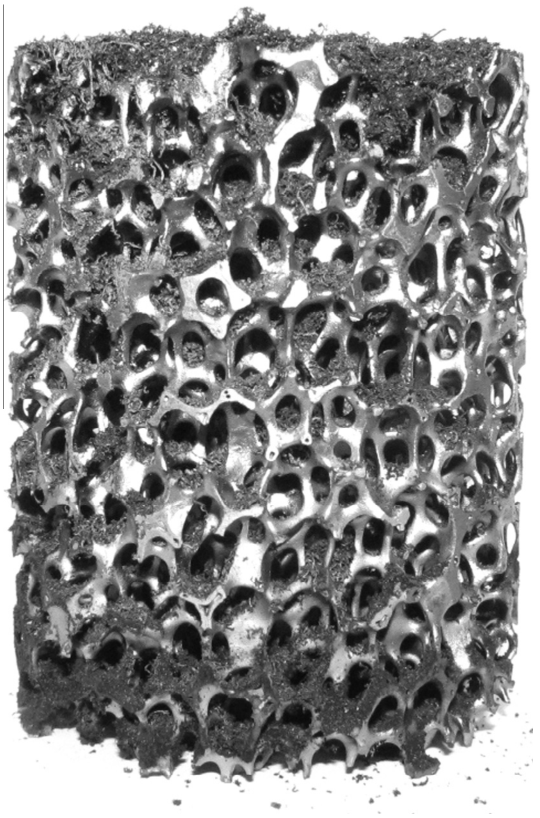

Fig. 7. The 50 mm tall RPC after one of the A experiments. The particles are uniformly distributed throughout the entire RPC.

and a small sample size. The reasons for the generally low carbon conversion may be attributed to insufficient solids retention or particle build up on top of the RPC that was observed in some experiments.

The upgrade factor calculated via Eq. (3) was found to be ~1.05 for cases A and B and less than 1 for PP and SG. This means that the biomass could be energetically upgraded by 5% by storing solar energy in the syngas.

Fig. 7 shows the RPC after one of the A experiments. The easily removable char particles were quite uniformly distributed throughout the entire structure, thereby implying rather volumetric char gasification. It was possible to feed up to 77 g/h bagasse without a significant increase in the pressure drop over the RPC. This corresponds to a particle flux per cross-sectional area of 16 g/s m^2. At higher feeding rates char started depositing on top of the RPC. The elemental analysis of the solid residue showed lower carbon conversion for particles collected in the product collection drum than for the particles retrieved from the RPC. This implies that the retention of the particles by the RPC and/or their interaction with the RPC surface is the key for increasing the overall carbon conversion.

The energy conversion efficiency is defined as

$$\eta = \frac{m_{\text{syngas}}\text{LHV}_{\text{syngas}}}{\int_{t_0}^{t_{\text{end}}} \dot{Q}_{\text{solar}}\, dt + m_{\text{bagasse}}\text{LHV}_{\text{bagasse}} - m_{\text{C,in}}(1 - X_{\text{C}})\text{LHV}_{\text{char}}} \tag{5}$$

η strongly depends on the feeding rate. For reporting the maximum η it is thus important to consider only the experiments in which no particle build-up was observed. Under this constraint, the highest efficiency of $\eta = 21.6\%$ was achieved at a feeding rate of 73 g/h (experiment A3). To overcome the throughput constraints and increase η it is necessary to develop a method for on-line ash removal from the RPC and improve the control of the solids residence time. Since the particles deposited on the RPC were easy to remove, vibration and/or occasional pulse-flow of purge gas (inert or syngas) could serve as means for achieving both of these tasks that should be addressed by further research.

4. Conclusions

A two-zone solar-driven biomass gasifier concept has been proposed and evaluated at a 1.5 kW_{th} solar radiative power input with bagasse particles. Its first zone operates in a drop-tube mode which ensures efficient radiative heat transfer to dispersed biomass particles that is required for fast pyrolysis. Its second zone is designed to operate as a trickle bed consisting of a structured packing that increases solids holdup in the hot zone, thereby providing residence time and temperature needed for the rate limiting char gasification and the decomposition of the pyrolysis products.

A series of 20 min gasification experiments with bagasse particles and steam were performed on a high-flux solar simulator to compare the drop-tube/trickle-bed reactor with a drop-tube reactor. It was demonstrated that the two-zone reactor concept decomposes CH_4 and C_2 hydrocarbons more efficiently than the drop-tube gasifier operating at comparable reactor tube temperatures. The concentrations of H_2 and CO_2 were higher than in the drop tube reactor, whereas the concentration of CO was lower, which has been attributed to a higher extent of the water–gas shift reaction due to a higher gas temperature.

The LHV of the syngas produced by the two-zone reactor was around 15.9 MJ/kg, which is substantially higher than typically obtained in conventional autothermal bagasse gasification. The biomass was energetically upgraded by 5%, effectively storing solar energy in the syngas. The maximum energy conversion efficiency was 21%.

It is important to note that the concept has only been evaluated under the very limited conditions of both short-term operation (20 min) and light particle loadings (a maximum particle flux of up to 16 g/s m^2 were achieved without particle build-up on the structure packing). Future research should address on-line ash removal from the structured packing to increase the throughput and ensure longer term operability.

Acknowledgments

We gratefully acknowledge the financial support by the Brazilian-Swiss Joint Research Programme (Grant Agreement No. BJRP 011005). We thank Mr. Alexander David for the assistance during the experimental campaign.

References

[1] Taylor RW, Berjoan R, Coutures JP. Solar gasification of carbonaceous materials. Sol Energy 1983;30:513–25.

[2] Piatkowski N, Wieckert C, Weimer A, Steinfeld A. Solar-driven gasification of carbonaceous feedstock—a review. Energy Environ Sci 2010;4:73–82.

[3] Bridgwater AV. The technical and economic feasibility of biomass gasification for power generation. Fuel 1995;74:631–53.

[4] Kruesi M, Jovanovic ZR, dos Santos EC, Yoon HC, Steinfeld A. Solar-driven steam-based gasification of sugarcane bagasse in a combined drop-tube and fixed-bed reactor – Thermodynamic, kinetic, and experimental analyses. Biomass and Bioenergy 2013;52:173–83.

[5] Z'Graggen A, Haueter P, Trommer D, Romero M, De Jesus J, Steinfeld A. Hydrogen production by steam-gasification of petroleum coke using concentrated solar power – II. Reactor design, testing, and modeling. Int J Hydrogen Energy 2006;31:797–811.

[6] Z'Graggen A, Haueter P, Maag G, Vidal A, Romero M, Steinfeld A. Hydrogen production by steam-gasification of petroleum coke using concentrated solar power–III. Reactor experimentation with slurry feeding. Int J Hydrogen Energy 2007;32:992–6.

[7] Z'Graggen A, Haueter P, Maag G, Romero M, Steinfeld A. Hydrogen production by steam-gasification of carbonaceous materials using concentrated solar energy–IV. Reactor experimentation with vacuum residue. Int J Hydrogen Energy 2008;33:679–84.

[8] von Zedtwitz P, Steinfeld A. Steam-gasification of coal in a fluidized-bed/packed-bed reactor exposed to concentrated thermal radiation – modeling and experimental validation. Ind Eng Chem Res 2005;44:3852–61.

[9] Trommer D, Noembrini F, Fasciana M, Rodriguez D, Morales A, Romero M, et al. Hydrogen production by steam-gasification of petroleum coke using concentrated solar power – I. Thermodynamic and kinetic analyses. Int J Hydrogen Energy 2005;30:605–18.

[10] Müller R, von Zedtwitz P, Wokaun A, Steinfeld A. Kinetic investigation on steam gasification of charcoal under direct high-flux irradiation. Chem Eng Sci 2003;58:5111–9.

[11] Gregg DW, Taylor RW, Campbell JH, Taylor JR, Cotton A. Solar gasification of coal, activated carbon, coke and coal and biomass mixtures. Sol Energy 1980;25:353–64.

[12] Murray JP, Fletcher EA. Reaction of steam with cellulose in a fluidized bed using concentrated sunlight. Energy 1994;19:1083–98.

[13] Piatkowski N, Steinfeld A. Solar-driven coal gasification in a thermally irradiated packed-bed reactor. Energy Fuels 2008;22:2043–52.

[14] Lichty P, Perkins C, Woodruff B, Bingham C, Weimer A. Rapid high temperature solar thermal biomass gasification in a prototype cavity reactor. J Sol Energy Eng 2010;132:011012.

[15] Perkins C, Jovanovic Z, Strand S, Hilton C, Kelley D. Systems and methods for an indirect radiation driven gasifier reactor & receiver configuration. In: Sundrop Fuels, Inc. US 2010/0303692 A1; 2010.

[16] Lede J, Verzaro F, Antoine B, Villermaux J. Flash pyrolysis of wood in a cyclone reactor. Chem Eng Process: Process Intensification 1986;20:309–17.

[17] Piatkowski N, Wieckert C, Steinfeld A. Experimental investigation of a packed-bed solar reactor for the steam-gasification of carbonaceous feedstocks. Fuel Process Technol 2009;90:360–6.

[18] Melchior T, Perkins C, Lichty P, Weimer AW, Steinfeld A. Solar-driven biochar gasification in a particle-flow reactor. Chem Eng Process: Process Intensification 2009;48:1279–87.

[19] Melchior T, Steinfeld A. Radiative transfer within a cylindrical cavity with diffusely/specularly reflecting inner walls containing an array of tubular absorbers. J Sol Energy Eng 2008;130. 021013-021013.

[20] Melchior T, Perkins C, Weimer AW, Steinfeld A. A cavity-receiver containing a tubular absorber for high-temperature thermochemical processing using concentrated solar energy. Int J Therm Sci 2008;47:1496–503.

[21] Maag G, Steinfeld A. Design of a 10 MW particle-flow reactor for syngas production by steam-gasification of carbonaceous feedstock using concentrated solar energy. Energy Fuels 2010;24:6540–7.

[22] Z'Graggen A, Steinfeld A. Hydrogen production by steam-gasification of carbonaceous materials using concentrated solar energy – V. Reactor

modeling, optimization, and scale-up. Int J Hydrogen Energy 2008;33:5484–92.

[23] Svoboda K, Pohořelý M, Hartman M, Martinec J. Pretreatment and feeding of biomass for pressurized entrained flow gasification. Fuel Process Technol 2009;90:629–35.

[24] Rensfelt E, Blomkvist G, Ekström C, Engström S, Espents B, Linnanki L. Basic gasification studies for development of biomass medium-BTU gasification processes. In: Energy from biomass and wastes. Washington (DC); 1978: p. 465–94.

[25] Shafizadeh F. Introduction to pyrolysis of biomass. In: Diebold J. (ed.) Specialists' workshop on fast pyrolysis of biomass. Copper Mountain (CO): Solar Energy Research Institute; 1980: p. 79–103.

[26] Fushimi C, Araki K, Yamaguchi Y, Tsutsumi A. Effect of heating rate on steam gasification of biomass. React Char Ind Eng Chem Res 2003;42:3922–8.

[27] Zanzi R, Sjöström K, Björnbom E. Rapid high-temperature pyrolysis of biomass in a free-fall reactor. Fuel 1996;75:545–50.

[28] Mermoud F, Salvador S, Van de Steene L, Golfier F. Influence of the pyrolysis heating rate on the steam gasification rate of large wood char particles. Fuel 2006;85:1473–82.

[29] Milosavljevic I, Oja V, Suuberg EM. Thermal effects in cellulose pyrolysis: Relationship to char formation processes. Ind Eng Chem Res 1996;35:653–62.

[30] Stubington JF, Aiman S. Pyrolysis kinetics of bagasse at high heating rates. Energy Fuels 1994;8:194–203.

[31] Zhang Y, Kajitani S, Ashizawa M, Miura K. Peculiarities of rapid pyrolysis of biomass covering medium- and high-temperature ranges. Energy Fuels 2006;20:2705–12.

[32] Zhang Y, Kajitani S, Ashizawa M, Oki Y. Tar destruction and coke formation during rapid pyrolysis and gasification of biomass in a drop-tube furnace. Fuel 2010;89:302–9.

[33] Steinfeld A, Palumbo R. Solar Thermochemical Process Technology. In: Robert AM, editor. Encyclopedia of Physical Science and Technology (3rd ed.). New York: Academic Press; 2003. p. 237–56.

[34] Hischier I, Leumann P, Steinfeld A. Experimental and numerical analyses of a pressurized air receiver for solar-driven gas turbines. J Sol Energy Eng 2012;134:021003–8.

[35] Welford WT, Winston R. High collection nonimaging optics. San Diego: Academic Press; 1989.

[36] Petrasch J, Coray P, Meier A, Brack M, Haberling P, Wuillemin D, et al. A novel 50 kW 11,000 suns high-flux solar simulator based on an array of xenon arc lamps. J Sol Energy Eng 2007;129:405–11.

[37] Natarajan E, Öhman M, Gabra M, Nordin A, Liliedahl T, Rao AN. Experimental determination of bed agglomeration tendencies of some common agricultural residues in fluidized bed combustion and gasification. Biomass and Bioenergy 1998;15:163–9.

[38] Turn SQ, Jenkins BM, Jakeway LA, Blevins LG, Williams RB, Rubenstein G, et al. Test results from sugar cane bagasse and high fiber cane co-fired with fossil fuels. Biomass and Bioenergy 2006;30:565–74.

[39] Demirbas A, Gullu D, Çaglar A, Akdeniz F. Estimation of calorific values of fuels from lignocellulosics. Energy Sources 1997;19:765–70.

[40] Grubbs FE. Procedures for detecting outlying observations in samples. Technometrics 1969;11:1–21.

[41] Roine A. Outokumpu HSC Chemistry. Pori (Finland): Outokumpu Research; 1997.

[42] Gabra M, Pettersson E, Backman R, Kjellström B. Evaluation of cyclone gasifier performance for gasification of sugar cane residue–Part 1: gasification of bagasse. Biomass and Bioenergy 2001;21:351–69.

[43] Erlich C, Fransson TH. Downdraft gasification of pellets made of wood, palm-oil residues respective bagasse: Experimental study. Appl Energy 2011;88:899–908.